Hydrogen storage in CO_2-activated amorphous nanofibers and their monoliths

M. Kunowsky[a], J.P. Marco-Lozar[a], A. Oya[b], A. Linares-Solano[a,*]

[a] Grupo de Materiales Carbonosos y Medio Ambiente, Departamento de Química Inorgánica, Universidad de Alicante, Ap. 99, E-03080 Alicante, Spain

[b] Graduate School of Engineering, Gunma University, Gunma 376-8515, Japan

Abstract

Amorphous carbon nanofibers (CNFs), produced by the polymer blend technique, are activated by CO_2 (ACNFs). Monoliths are synthesized from the precursor and from some ACNFs. Morphology and textural properties of these materials are studied. When compared with other activating agents (steam and alkaline hydroxides), CO_2 activation renders suitable yields and, contrarily to most other precursors, turns out to be advantageous for developing and controlling their narrow microporosity (< 0.7 nm), $V_{DR}(CO_2)$. The obtained ACNFs have a high compressibility and, consequently, a high packing density under mechanical pressure which can also be maintained upon monolith synthesis. H_2 adsorption is measured at two different conditions (77 K / 0.11 MPa, and 298 K / 20 MPa) and compared with other activated carbons. Under both conditions, H_2 uptake depends on the narrow microporosity of the prepared ACNFs. Interestingly, at room temperature these ACNFs perform better than other activated carbons, despite their lower porosity developments. At 298 K they reach a H_2 adsorption capacity as high as 1.3 wt.%, and a remarkable value of 1 wt.% in its mechanically resistant monolith form.

* Corresponding author. Tel: +34 965 90 3545. Fax: +34 965 90 3454. E-mail address: linares@ua.es (A. Linares-Solano)

1. Introduction

Carbon nanofibers (CNFs) are currently investigated for a wide range of energy related applications such as electrodes in fuel cells [1-3], batteries [3, 4], and supercapacitors [3, 5-8], as catalyst support [9, 10], or sensors [11, 12]. Another promising application for CNFs is hydrogen storage [13-24]. Some early works claimed groundbreaking results which generated an important interest in this field [14, 15]. However, these results could not be reproduced by other research groups [13, 17, 18].

For systems in which the hydrogen molecule is physisorbed on the surface of the adsorbent, porosity remains a crucial parameter [24]. Porous carbon materials can have different morphologies (e.g. powder, pellets, fibers, cloths, etc.). Activated carbon fibers (ACFs), a type of activated carbon with fibrous morphology and diameter around 10 µm, offer a number of advantages over conventional activated carbons [25]. For example, their fibrous structure is beneficial for developing microporosity upon activation, which is directly accessible and provides higher adsorption rates [26]. The mentioned characteristics can be further improved by reducing the fiber cross-section. Carbon nanofibers (CNFs) usually have diameters between 5 and 500 nm, and these nanosized dimensions make them interesting candidates for numerous applications [8, 26]. They can be synthesized using different methods, most of them being prepared by catalytic chemical vapor deposition (CVD), using hydrocarbon as carbon source [9, 26]. Unfortunately, their graphitic structure and crystal order impede their subsequent activation and the reaching of a suitable porosity development [20, 22, 27].

Fortunately, CNFs with lower crystal order can be developed by other preparation

processes, for example by polymer blend technique [28, 29], by electrospinning [21, 30,31], or by template carbonization technique [32]. Recently, a novel kind of CNFs, produced by polymer blend technique and mechanical spinning, has been used for producing highly nanoporous ACNFs adsorbents [5, 6, 8, 22]. In difference to CNFs synthesized by other methods, the CNF-precursors feature a highly amorphous structure which substantially favors their activation [22]. From these nanofibers, Shiraishi et al. synthesized ACNFs with high surface areas up to 2000 m^2g^{-1} by physical activation with H_2O [5, 6]. However, very low activation yields of only 6 wt.% were reached [5, 6]. Suárez-García et al. obtained highly microporous adsorbents with BET surface areas of more than 1700 m^2g^{-1} and significantly higher yields by chemical activation with hydroxides [22].

In the present work, our main objective is to analyze the synthesis of highly microporous ACNFs with high yields by a CO_2 activation process, which has not been performed before for these CNFs and is much less laborious and costly than hydroxide activation. The obtained results confirm the advantage of the highly amorphous character of the pristine CNFs, being beneficial for their activation process. Furthermore, nanofiber monoliths are produced from the investigated materials in order to increase their density. The morphologies and textural properties of the produced materials are studied, and their application as hydrogen storage materials is investigated. The hydrogen adsorption measurements are conducted in verified automated devices which ensure high reproducibility.

2. Experimental

2.1 Sample preparation

The carbon nanofibers were obtained by using a combination of polymer blend technique and spinning [28, 29]. For this purpose, a novolac-type phenolic resin (PR) (Gun-ei Chemical Ind. Co. Ltd., Japan) was used as carbon precursor, and a high density polyethylene (PE) (Idemitsu Petrochemical Ind. Co. Ltd., Japan) as pyrolyzing polymer. A mixture of both polymers (PR/PE=1/9) was blended mechanically at 443-473 K, followed by continuous melt spinning at 423-473 K. Afterwards, the resulting fibers were stabilized in acid solution, neutralized, washed and dried at room temperature under vacuum. The stabilized blend fibers were soaked in toluene held around the boiling point to remove the matrix PE. Finally stabilized PR nanofibers recovered were carbonized at 950 K for 0.5 h under N_2 atmosphere, producing bundles of several hundred of carbon fibers with nanometric size diameters. Further details of this procedure have been reported in the literature [28, 29].

In the present work, physical activation of the CNFs with CO_2 was performed in a horizontal tube furnace. Firstly, the nanofibers were heated under a N_2 flow of 100 ml min^{-1} with a rate of 20 K min^{-1}. Upon reaching the activation temperature of 1098 K, the flow was switched to CO_2 (100 ml min^{-1}). Different activation times of 12 h, 24 h, and 32 h were used. For comparison purposes, results obtained with other activating agents such as steam and hydroxides (NaOH and KOH) are used which are described elsewhere [5, 6, 8, 22]. About the nomenclature used for the activated samples, this follows the form ACNF-[X][Y]. Thereby, [X] corresponds to the activating agent used, being “CD” in the case of carbon dioxide, “S” for steam, “Na” for sodium [Y]

hydroxide, and finally "K" for potassium hydroxide. For physically activated samples, corresponds to the activation time in hours, whereas for chemically activated samples [Y] indicates the hydroxide/CNF ratio.

Monoliths were prepared by mixing of the nanofibers with a commercially available aqueous solution of polymeric binder (polyvinyl dichloride PVDC, 55 %) (Waterlink Sutcliffe Carbons) in a 1/1 PVDC/fiber ratio (weight basis). The mixture was dried for 24 h at 323 K and compressed in a mould, applying a pressure of 259 MPa. Then the mould was heated with a ramp of 10 K min^{-1} up to 413 K. Finally, the resulting monolith was heated under a nitrogen flow of 100 ml min^{-1} in order to carbonize the binder. Thereby, a heating rate of 2 K min^{-1} was used, and the temperatures were maintained constant for 1 h at 448 K, 1 h at 723 K, and 2 h at the final temperature of 1023 K. With the purpose of comparing the obtained results, monoliths were prepared from both, the original CNFs, and for intermediate ACNFs (ACNF-CD24). According to their precursors, the monoliths are denominated CNF-M, and ACNF-CD24-M, respectively. A detailed description of the monolith preparation procedure can be found in Reference [33].

2.2 Characterization methods

Porous texture characterization of all the samples was carried out by the physical adsorption of gases (N_2 at 77 K and CO_2 at 298 K), using an automatic adsorption system (Micromeritics ASAP 2020). Previous to the adsorption measurements, the samples were degassed at 523 K under vacuum for at least 4 h. From N_2 adsorption isotherms, the DFT pore size distributions and the apparent BET surface area (S_{BET})

were obtained, and the total micropore volume ($V_{DR}(N_2)$) was calculated according to the Dubinin–Radushkevich (DR) equation. The DR equation was also applied to CO_2 adsorption isotherms, in order to determine the volume of narrow micropores ($V_{DR}(CO_2)$) for pores with mean pore sizes lower than 0.7 nm.

Packing densities, ρ, of the CNFs-materials were measured by using a mechanical press. A given amount of sample (0.5 g approx.) was introduced into a cylindrical steel mould with a diameter of 13 mm. In order to compact the sample, a mechanical pressure of 73.9 MPa was applied on the sample with a steel cylinder. The volume occupied by the sample was evaluated by measuring the penetration depth of the steel cylinder in comparison with a reference measurement in which no sample was introduced into the mould. Two different packing density values were measured. The first value, ρ_p, was obtained while mechanical pressure was maintained on the sample. The second value, ρ_r, was measured after the pressure was released. Piece densities of monoliths, ρ_m, were obtained by measuring their dimensions and weights. The obtained densities have an error smaller than 3 % [33].

To observe possible changes in the morphology of the carbon nanofibers after the activation process, scanning electron microscopy (SEM) studies were carried out with a JEOL JSM-840 microscope with 20 kV acceleration voltage.

In order to determine the appropriate selection of the activation temperature for the physical activation with CO_2, the CNFs' reactivity was estimated under carbon dioxide atmosphere. Reactivity in CO_2 was analyzed at different temperatures by thermogravimetric analysis (TG), heating the sample in He (100 ml min^{-1}) with a rate of

20 K min^{-1}. Upon reaching the desired temperature, the flow was switched to CO_2 (100 ml min^{-1}).

2.3 H_2 adsorption measurements

Hydrogen adsorption was measured at different conditions of pressure and temperature (at 77 K and sub-atmospheric pressures, and at room temperature up to 20 MPa) in different devices. At 77 K, hydrogen adsorption capacities were measured in an automatic volumetric adsorption apparatus (Micrometitics ASAP 2020). For each experiment, approximately 0.1 g of sample was degassed at 523 K for 4 h under vacuum.

At room temperature, measurements were carried out on selected samples at 298 K with pressures up to 20 MPa. For these measurements, a fully automated volumetric apparatus, designed and built up at University of Alicante, was used [34]. This device has been used for a number of earlier studies on hydrogen adsorption in our group, ensuring high comparability of the obtained results [24, 27, 35-37]. Previous to each measurement, the sample was heated at 423 K for 4 h under vacuum. The weight of the degassed sample was measured, being around 0.5 g in the case of all measurements. After that, the sample was located in the sample volume, where it was degassed again at 423 K during another 4 h in vacuum, in order to prepare the sample for the measurement. The device was regularly tested for leaks, and the reference volume (< 19 cm^3) was determined with a calibrated volume. The volume on the sample side was determined with helium gas before each measurement and ranged between 20.1 and

22.4 cm^3. The reference temperature was maintained at 308 K, while the sample volume temperature of 298 K was controlled by a thermostat with cooling liquid.

3. Results and discussion

3.1 Thermogravimetry

Thermogravimetric analysis (TG) was performed as an indication of the precursor's carbon dioxide reactivity to select the most convenient activation temperature to be used for the activation process of the CNFs. These TG measurements were performed by heating the CNF-precursor under N_2 atmosphere (100 ml min^{-1}) with a rate of 20 K min^{-1} up to a given temperature (1073 K, 1098 K and 1123 K). Once the final temperature was reached, the flow was switched to CO_2 (100 ml min^{-1}) and the weight loss was recorded. Figure 1 summarizes the TG curves corresponding to the three temperatures analyzed. The weight loss decreases constantly over the time studied and, as expected, an increase in the temperature provokes a faster weight loss. Finally, the intermediate temperature (1098 K) was chosen for the activation experiments, in order to reach suitable activation degrees in convenient periods of time to control and to develop the CNFs porosity.

3.2 Textural properties and morphology

The N_2 adsorption isotherms at 77 K of the pristine CNFs and the CO_2 activated samples are plotted in Figure 2a and their corresponding pore size distributions in

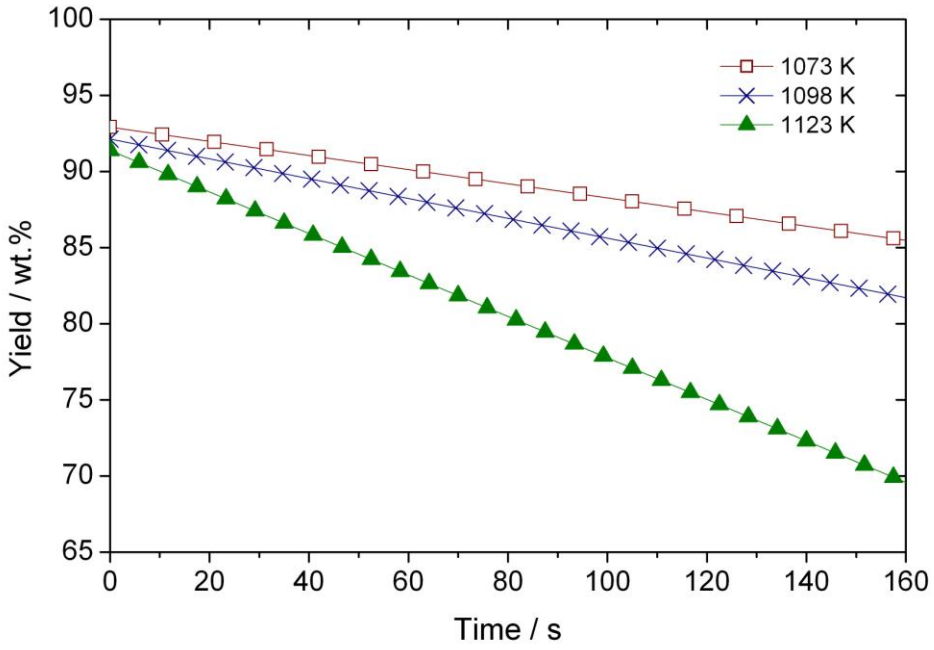

Figure 1. TG curves in CO_2 at different temperatures for the original CNFs.

Figure 2b. For comparison purposes, Figure 2c plots the N_2 adsorption isotherms of some ACNFs prepared using different KOH/CNFs ratios [8, 22]. From the shapes of the isotherms in Figure 2a it can be concluded that all of the materials are essentially microporous. With the activation time, the adsorption capacity of the samples increases (see Figures 2a and 2b), starting to possess, as indicated by the steep rise at low P/P_0 values, some mesoporosity (large mesopores) and well developed macroporosity. It can be observed that during the first 12 hours of activation, the development of porosity is mainly focused on the microporosity region which increases considerably. Until 24 hours, the microporosity continues to rise and mesopores appear. Interestingly, the microporosity is only slightly affected for longer activation times. Thus, a widening of the existing porosity can be observed for the sample that was activated for 32 hours, as it can clearly be seen in Figure 2b.

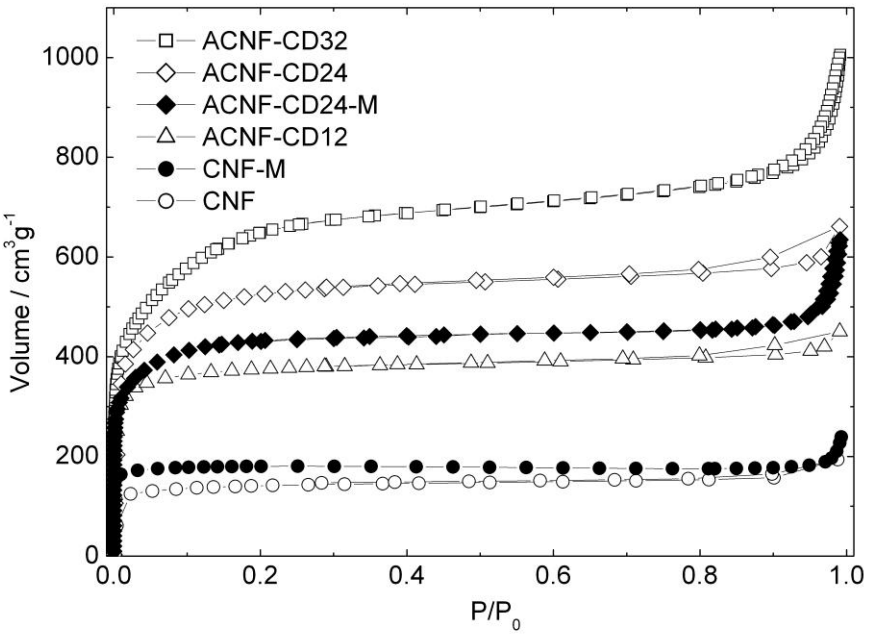
ACNF-CD32
ACNF-CD24
ACNF-CD24-M
ACNF-CD12
CNF-M
CNF
Volume / cm3g-1
P/P0
0
200
400
600
800
1000
0.0
0.2
0.4
0.6
0.8
1.0

(a)

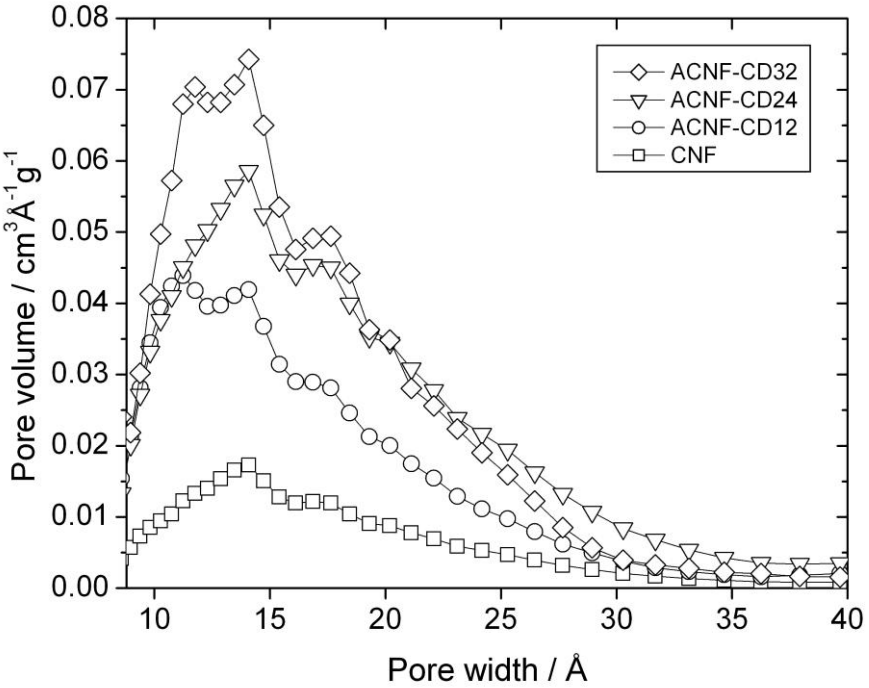
ACNF-CD32
ACNF-CD24
ACNF-CD12
CNF
Pore volume / cm3Å-1g-1
Pore width / Å
0.00
0.01
0.02
0.03
0.04
0.05
0.06
0.07
0.08
10
15
20
25
30
35
40

(b)

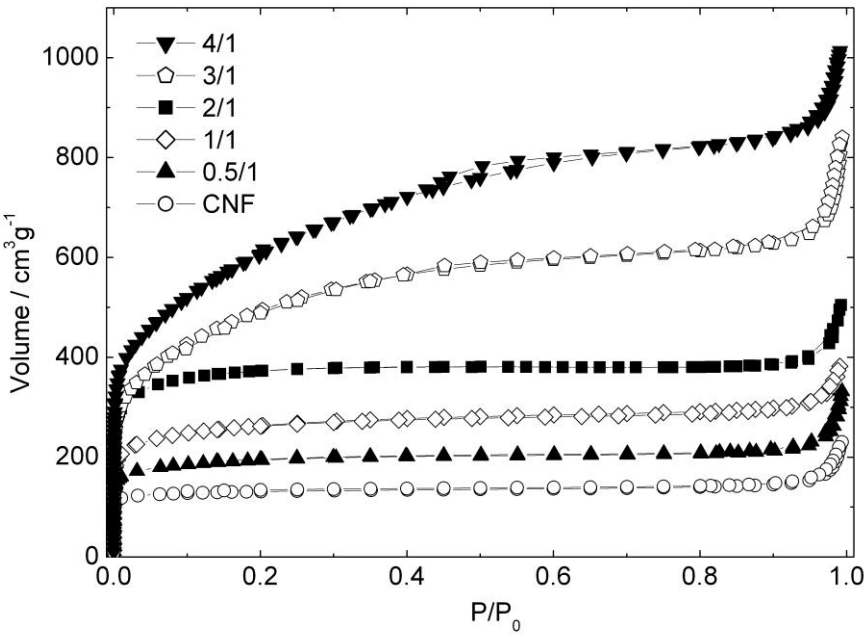

(c)

Figure 2. N_2 adsorption isotherms of the original CNFs, ACNFs, and monoliths that were produced by (a) physical activation with CO_2, (b) their pore size distribution (DFT method) and (c) the ACNFs chemically activated with KOH (in part obtained from Suárez-García et al. [22], and Barranco et al. [8]).

Figure 2c shows the activation results for CNFs using five KOH/CNFs ratios (from 0.5 to 4/1). Similar results (but with lower yields, not shown here) are obtained when these CNFs are activated with NaOH [22]. Both, their amorphous character and their important initial microporosity, facilitate their activation and the development of porosity. The isotherm shapes of Figure 2c (all type I) show that all of the samples are microporous and that the hydroxide/CNFs ratio has a strong influence on the porosity development. Thus, it can be observed that the microporosity widens with increasing ratios, confirming previous results [38]. A comparative observation of Figures 2a, 2b

and 2c allows to see that: i) both activating agents develop very well the adsorption capacity of these CNFs and ii) for the most developed ACNFs, the resulting pore size distributions are more homogeneous in the case of CO_2 (much narrowed isotherm knee and horizontal isotherm plateau) than with KOH (much widening of the isotherm knee and much slope of the isotherm which both indicate of having a much heterogeneous and wider pore size distribution).

From gas adsorption isotherms (N_2 at 77 K and CO_2 at 298 K), the apparent BET surface area (S_{BET}), as well as the micropore volumes for the total ($V_{DR}(N_2)$), and the narrow ($V_{DR}(CO_2)$) microporosity were calculated. The porosity characterization is listed together with the activation yields and material densities in Table 1. For comparison purposes, Table 1 also includes the characterization results of samples obtained from steam activation [5, 6] and from chemical activation [8, 22]. For the ACNFs, the activation conditions can be deduced from their denomination, as it was explained earlier in Section 2.

The interesting starting porosity of the CNFs precursor, that reaches an apparent S_{BET} value of 520 m^2g^{-1}, can further be well developed. Thus, activated samples with a wide variety of adsorption capacities and micropore size distributions can be obtained by any of the activation methods used (CO_2, steam, KOH or NaOH). All of these activation methods allow to reach S_{BET} higher than 2000 m^2g^{-1}. A closer look to the results in Table 1 shows that: i) the $V_{DR}(CO_2)$ values, related to the micropore lower than 0.7 nm, are much higher for CO_2 activated CNFs, revealing a narrower micropore size distribution, and ii) for comparable porosity developments (e.g. similar S_{BET}) the activation yield has to be considered. In physically activated samples it can be seen that

Table 1. Characterization results of the original CNFs and the ACNFs.

Sample	S_{BET} [m^2g^{-1}]	$V_{DR}(N_2)$ [cm^3g^{-1}]	$V_{DR}(CO_2)$ [cm^3g^{-1}]	Yield [wt.%]	Packing densities [g cm^{-3}]	
					ρ_p [a]	ρ_r [b]
CNF	520	0.22	0.26	---	0.78	0.33
ACNF-K0.5 [8]	757	0.33	0.28	55	---	---
ACNF-K1 [8]	1070	0.47	0.35	20*	---	---
ACNF-K2 [8]	1378	0.64	0.52	35	---	---
ACNF-K3 [22]	1765	0.68	0.45	30	---	---
ACNF-Na3 [22]	1515	0.60	0.40	17	---	---
ACNF-S1 [5, 6]	1010	0.40	---	14	---	---
ACNF-S3 [5, 6]	1760	0.72	---	7	---	---
ACNF-S5 [5, 6]	2010	0.78	---	6	---	---
ACNF-CD12	1240	0.60	0.53	59	0.64	0.21
ACNF-CD24	1910	0.87	0.59	30	0.49	0.21
ACNF-CD32	2260	0.91	0.57	13	0.47	0.16

[a] under pressure
[b] after pressure release
* the expected value should be around 40; during the washing process the sample nanosize and the small amount of sample used, could cause a wrong low carbon yield.

CO_2 activation is clearly advantageous over steam. Figure 3 highlights this fact, comparing the activation yield of physically activated CNFs (steam and CO_2) over the apparent S_{BET}. The diagram shows that, in order to gain similar porosity developments (i.e. 2000 m^2g^{-1}), the activation yield obtained with steam is around 6 % whereas for CO_2 activation a yield of 30 % is achieved. The activation rate used for steam [5, 6] was much higher than the one used for CO_2, as a result of which a poorer (less selective) activation is obtained for a given carbon yield, rendering lower porosity and BET values.

Doing a similar comparative look with hydroxide activation, it can be concluded that physical activation with CO_2 is also more efficient than hydroxide activation, giving higher $V_{DR}(CO_2)$ and, in general, similar or higher activation yields. These observed

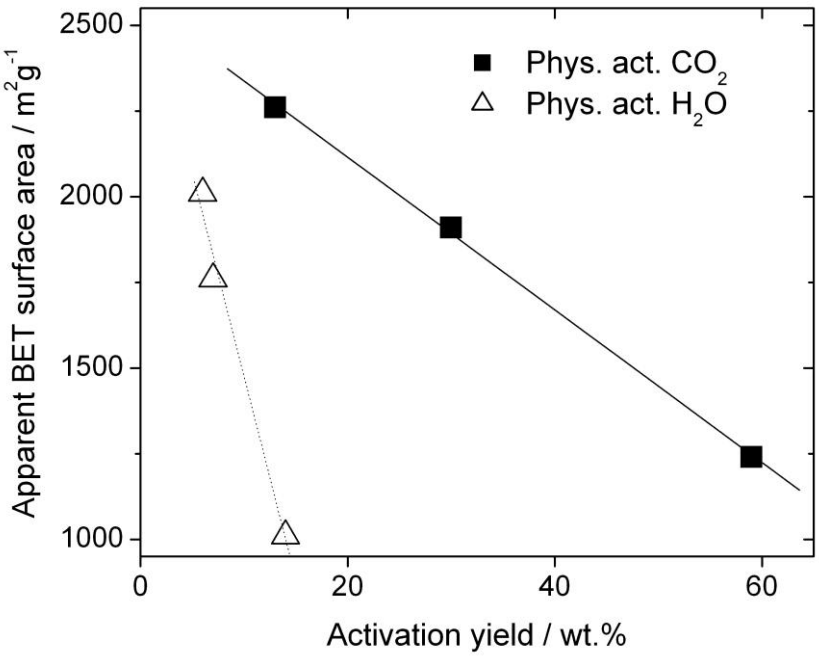

Figure 3. Comparison of different methods for physical activation of the CNFs. Results for physical activation with H_2O were taken from [5, 6].

differences among the activating agents used can be caused by their very different activation conditions (activation time, temperature, etc.) and their different chemical nature (gases: steam and CO_2; or hydroxides: NaOH and KOH). For these four activating agents, their carbon contact, their activation mechanism, as well as their activation process are too different [38]. Consequently, the pore structures of the resulting activated samples are different. Additionally, the performance of each activating agent is also closely related to the kind of precursor which is activated.

Interestingly, in the case of the amorphous CNFs investigated in this study, this precursor behaves differently to most other precursors, for which hydroxide activation was more selective to develop $V_{DR}(CO_2)$ than physical activation [38, 39].

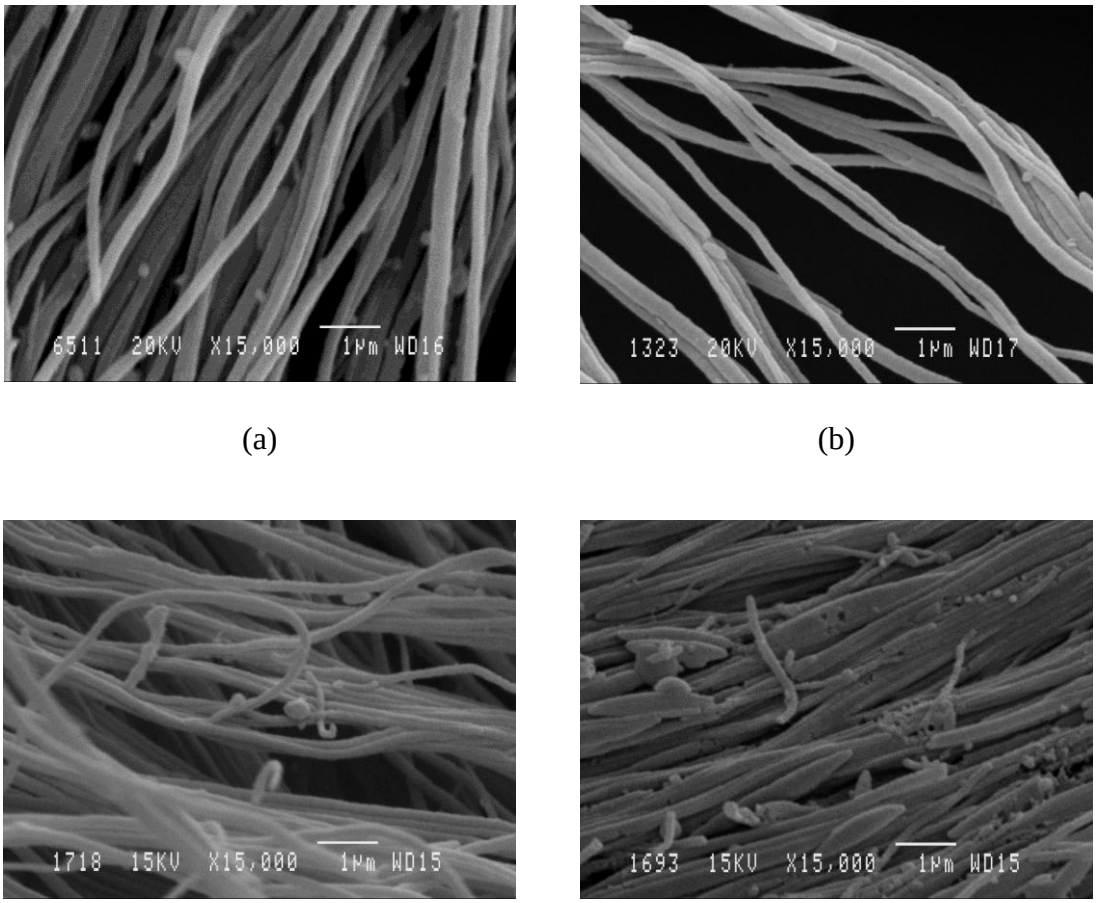

(a) (b)

(c) (d)

Figure 4. Scanning electron micrographs of the original sample and the physically activated CNF at different times. (a) Original CNF; (b) ACNF-CD12; (c) ACNF-CD24 and (d) ACNF-CD32.

In order to analyze possible modifications of the CNFs morphology due to the activation process, scanning electron microscopy (SEM) studies have been carried out.

Figure 4 shows SEM micrographs of the original and the ACNFs that were physically activated with CO_2 for 12 h, 24 h, and 32 h. From the obtained micrographs, it is important to point out that, in general, the physically ACNFs retain their fibrous morphology after activation, similar to what also happens in the case of hydroxide

activations [8, 22]. The fact that the fiber diameter is not affected by the activation process indicates that activation took place uniformly within the bulk of the fiber. Only for the highest activation time (32 h), the ACNFs present some imperfections in their structure.

3.3 Packing and monolith densities

For hydrogen storage application, the adsorbent has to be introduced into a tank with a given volume. Therefore, not only the textural properties but also the density of the adsorbent becomes very important [24, 27]. The higher the density, the higher will be the amount of adsorbent that can be comprised inside a certain volume. In Table 1, the values of the packing densities obtained from the pristine and the activated CNFs are listed. It can be seen that, under pressure, high packing densities ρ_p of 0.47 to 0.78 g cm^{-3} are reached. This high compressibility could make these ACNFs interesting candidates for hydrogen storage application. However, if the mechanical pressure is released, packing density values decrease drastically, reaching ρ_r values close to 0.2 g cm^{-3} for the activated samples. This resiliency behavior of the polymer blend CNFs, i.e. its tendency to recover its original state when the applied pressure is released, was also observed in a previous work [22]. Resiliency can be advantageous for different applications (e.g., as an electrode in a Li-ion battery) [4]. However, for their application to H_2 storage, this behavior is a technical problem that has to be solved.

Possible solutions for avoiding resiliency behavior and to increase the effective packing density values are: i) to maintain the packing pressure during the ACNFs tank filling

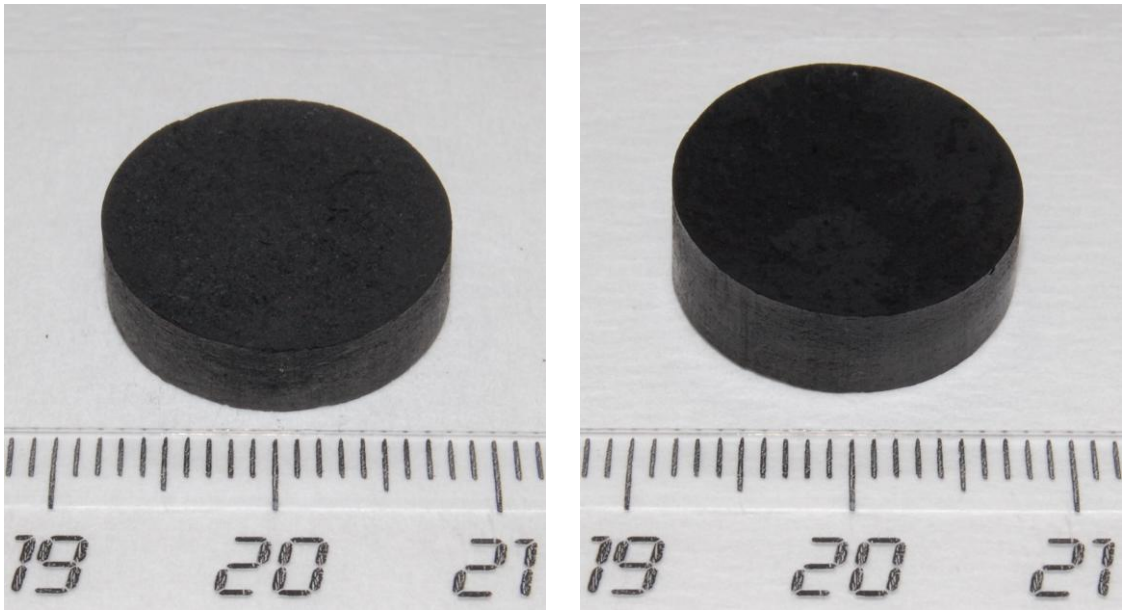

(a) (b)

Figure 5. Photographs of monoliths (a) CNF-M and (b) ACNF-CD24-M, synthesized from the original CNF and sample ACNF-CD24, respectively.

process, which can have technological difficulties and ii) to prepare carbon monoliths with these ACNFs [33]. In order to analyze this latter possibility, ACNFs which were activated with CO_2 for 24 h and also the original CNFs were used to prepare carbon monoliths. Both monoliths have a similar weight of approximately 0.5 g (degassed). In Figure 5, photographs of the synthesized monoliths are shown. It can be seen that they are solid, entire pieces, with suitable mechanical resistance and without mayor imperfections. Because both samples were prepared with similar weights, sample CNF-M (Figure 5a) presents a smaller piece volume (lower height) than the ACNF-CD24-M monolith (Figure 5b), confirming a lower density of the latter. Table 2 contains the packing/piece density values, ρ_r, and ρ_m, measured for the original CNFs, the ACNF-CD24 sample, and the corresponding monoliths (CNF-M and ACNF-CD24-M),

Table 2. Porous texture parameters and packing/piece densities ρ_r and ρ_m for the pristine CNFs, the ACNFs activated with CO_2 for 24 h and their monoliths.

Sample	S_{BET} [m^2g^{-1}]	$V_{DR}(N_2)$ [cm^3g^{-1}]	$V_{DR}(CO_2)$ [cm^3g^{-1}]	ρ_r and ρ_m [g cm^{-3}]
CNF	520	0.22	0.26	0.33
CNF-M	587	0.28	0.31	0.56
ACNF-CD24	1910	0.87	0.59	0.21
ACNF-CD24-M	1450	0.65	0.53	0.46

respectively. It can be seen that the densities of the materials could be significantly increased by monolith preparation. In the case of the pristine CNFs, the density rises a 70 %, while for the ACNF-CD24 sample the density is more than doubled. It is remarkable that for the latter, the monolith density reaches almost the ρ_p value of the compressed fiber, exposed to a mechanical pressure of 73.9 MPa (see Table 1). Table 2 also includes textural characterization of the prepared monoliths and their precursors. In the case of the original CNFs, monolith preparation develops a slightly higher porosity. On the contrary, the use of a binder for the preparation of the ACNFs monolith produces a decrease in the N_2 and CO_2 adsorption capacities. These observations are due to the additional porosity contribution of the carbonized binder which is higher than the unactivated CNFs, but lower than the porosity of the ACNFs.

3.4 Hydrogen adsorption

3.4.1 H_2 adsorption at low pressures and temperatures

It is important to recall that at 77 K and up to 0.11 MPa, hydrogen is adsorbed as a supercritical gas for which the concept of relative pressure (P/P_0, with P_0 being the

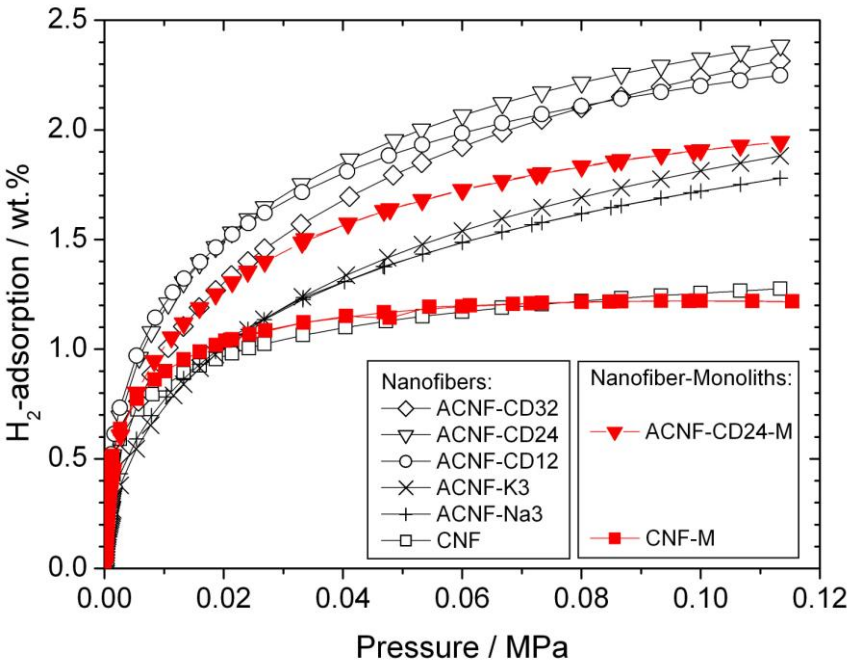

Figure 6. H_2 excess adsorption isotherms at 77 K and sub-atmospheric pressures on the pristine CNFs, the ACNFs activated physically with CO_2, the corresponding monoliths (filled symbols), as well as the ACNFs chemically activated with NaOH and KOH [22].

saturation pressure) cannot be used. However, a "relative pressure" calculated as "P/P_{CS}" could be used, with P_{CS} being calculated by the empirical equation proposed by Dubinin, as $P_{CS} = P_C(T/T_C)^2$ [40, 41]. Thereby, T_C and P_C are the critical temperature (33 K), and the critical pressure (1.3 MPa) of hydrogen. At these experimental adsorption conditions the calculated P_{CS} value is 7 MPa. Therefore, the "relative P/P_{CS}" range covered up to 0.11 MPa is very low (< 0.015), and hence, the type of the microporosity (size) being effective for H_2 adsorption is crucial, as it will be shown below.

Figure 6 presents the hydrogen adsorption isotherms at 77 K and sub-atmospheric pressures, expressed on gravimetric basis, for the CNF-precursor and for ACNFs

synthesized by physical activation with CO_2. The isotherms of the prepared monoliths are indicated by filled symbols. For comparison, also a selection of ACNFs prepared by hydroxide activations are shown in Figure 6, including KOH- and NaOH-activated samples with hydroxide/CNFs ratios of 3/1 [22].

The results of Figure 6 allow to point out several observations: i) as expected by its textural properties, the un-activated precursor already adsorbs an important amount ofH_2 (1.26 wt.%), ii) the hydrogen adsorption capacity increases significantly with the activation process following the order CNFs < ACNF-Na3 < ACNF-K3 < ACNF-CD12 < ACNF-CD32 < ACNF-CD24 and iii) although some relationship seems to exist between the sample S_{BET} and its hydrogen adsorption capacity, the key factor that controls the hydrogen uptake is its narrow micropore volume. This is confirmed in Figure 7, where the hydrogen uptake is plotted vs. the sample S_{BET} (Figure 7a) and vs. the narrow micropore volume (Figure 7b). Thus, the highest adsorption capacity of sample ACNF-CD24 (2.44 wt.%) does not correspond to the sample which has the highest S_{BET}, but with the sample with the highest $V_{DR}(CO_2)$ (see Table 1, $V_{DR}(CO_2)$ = 0.59 cm^3g^{-1}). Additionally, it can be seen from Figure 7b that the hydrogen uptake sequence follows very well the same trend as the narrow micropore volumes. In summary, at these experimental conditions (77 K and 0.11 MPa), the narrow microporosity plays the most relevant role in H_2 adsorption, due to its higher adsorption potential, explaining the correlation obtained between H_2 uptake and the narrow micropore volume. Such tendency is expected and in agreement with findings from the literature where similar relations were described [24, 27, 42].

For the monoliths, the hydrogen adsorption isotherms are represented in Figure 6 (filled symbols), together with those of their corresponding pristine materials (empty symbols).

As expected, no significant differences can be observed between the un-activated CNFs and its monolith CNF-M, since the narrow microporosity is quite similar for both samples. The ACNF-CD24-M monolith sample reaches a H_2 adsorption capacity which is similar to the powder ACNFs obtained by hydroxide activations, but lower than for parameters obtained for both materials, since the $V_{DR}(CO_2)$ of the monolith is slightly the ACNF-CD24 sample. This observation is in agreement with the porous texture decreased in comparison with its ACNFs precursor. Interestingly, the comparison of ACNF-CD24-M with samples having similar S_{BET} (see Table 1) shows that the monolith, in addition to its shape and its mechanical resistance, has a higher H_2 adsorption capacity than ACNFs samples in powdered form (see Figure 6).

Figures 7a and 7b show additional results obtained with activated carbon samples having different morphologies (powder) and size (activated carbon fibers with 10-20 μm) than the ACNFs studied in this work, in order to confirm the above observations. It can be observed that under these experimental conditions (77 K and 0.11 MPa) the $V_{DR}(CO_2)$ of the sample explains very well its hydrogen uptake (see Figure 7b), independently of its morphology and of its size; all the activated carbons plotted in Figure 7 follow the same general trend.

3.4.2 H_2 adsorption at high pressures and room temperature

For hydrogen storage at room temperature and up to 20 MPa the maximum P/P_{CS} value reached is < 0.19. As reported previously, the narrow microporosity of the sample will also control the storage capacity under these conditions [24, 27, 35]. Figure 8 presents

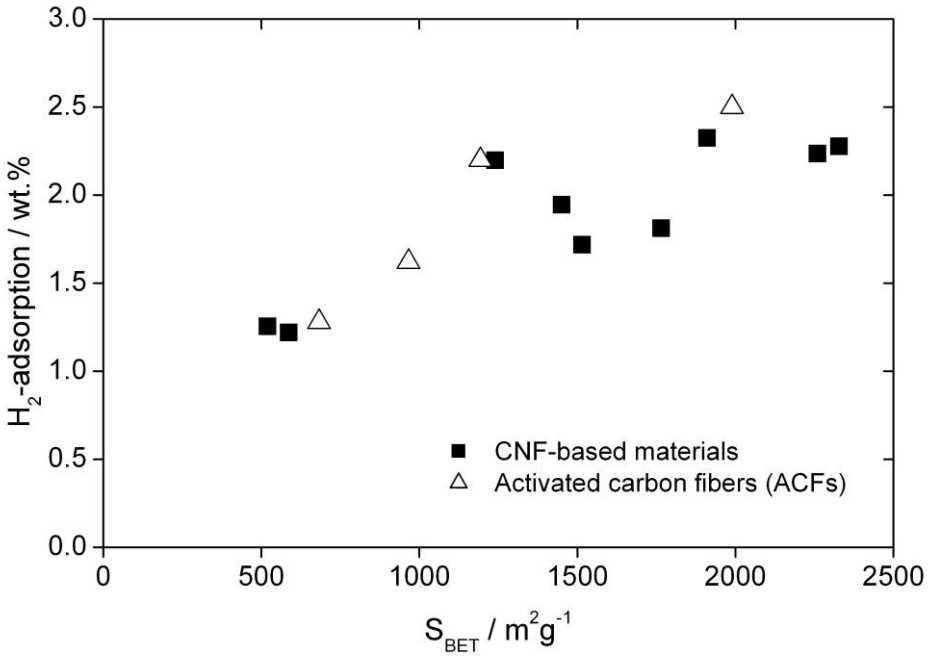

(a)

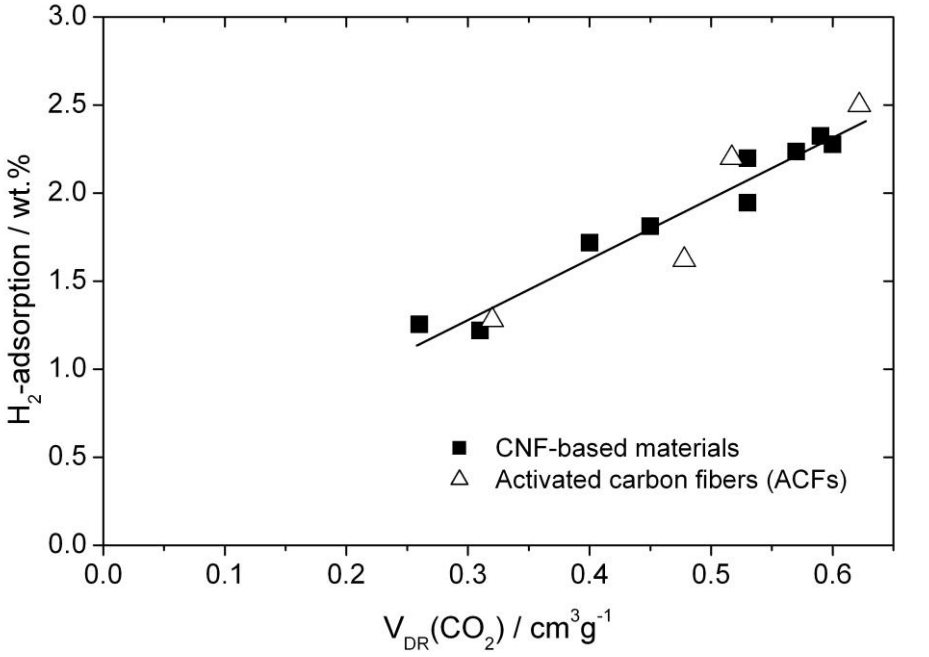

(b)

Figure 7. H_2 excess adsorption at 77 K and 0.11 MPa, plotted over (a) the apparent BET surface area, and (b) the narrow micropore volume. Measurements were performed for different carbon materials in the same device. Filled symbols indicate CNF-based samples investigated in this study, empty symbols correspond to conventional activated carbon fibers [27].

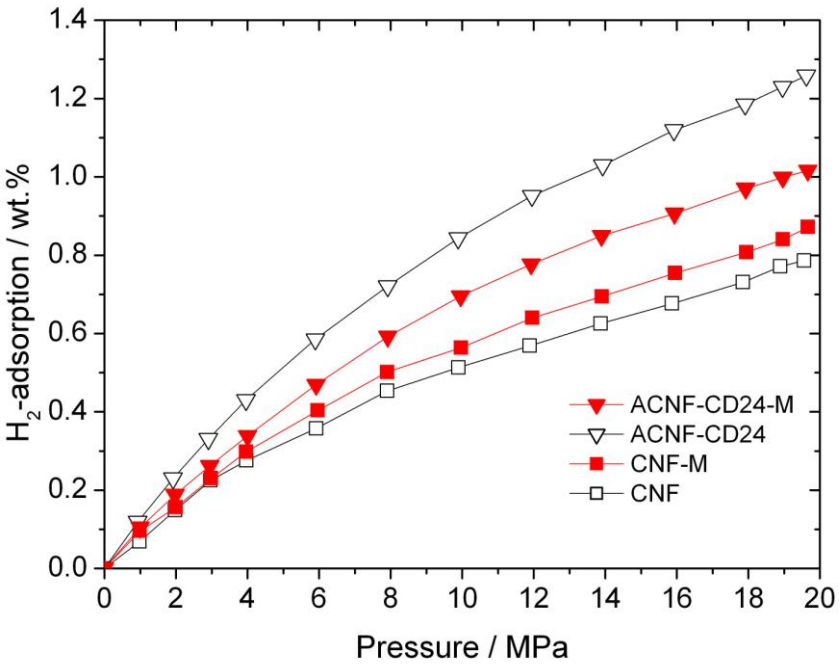

Figure 8. H_2 excess adsorption isotherms at 298 K for the original CNF, the ACNF activated with CO_2 for 24 h and their monoliths.

the H_2 adsorption results obtained at room temperature and at high pressures (up to 20 MPa) obtained for four samples: the two monoliths (ACNF-M and ACNF-CD24-M), and their corresponding precursors (CNFs and ACNF-CD24). As in the case of adsorption at 77 K, the un-activated CNFs already adsorb a considerable amount of hydrogen at room temperature and 20 MPa (over 0.8 wt.%). Comparing the original CNFs sample and its monolith, CNF-M, the latter presents a slightly higher H_2 uptake, because of its higher narrow microporosity ($V_{DR}(CO_2)$). Both ACNF samples (ACNF-CD24 and ACNF-CD24-M) present remarkable H_2 adsorption capacities (near 1.3 wt.% for ACNF-CD24 and over 1 wt.% for the monolith) which are related to their corresponding narrow microporosity developments. Under similar conditions (room

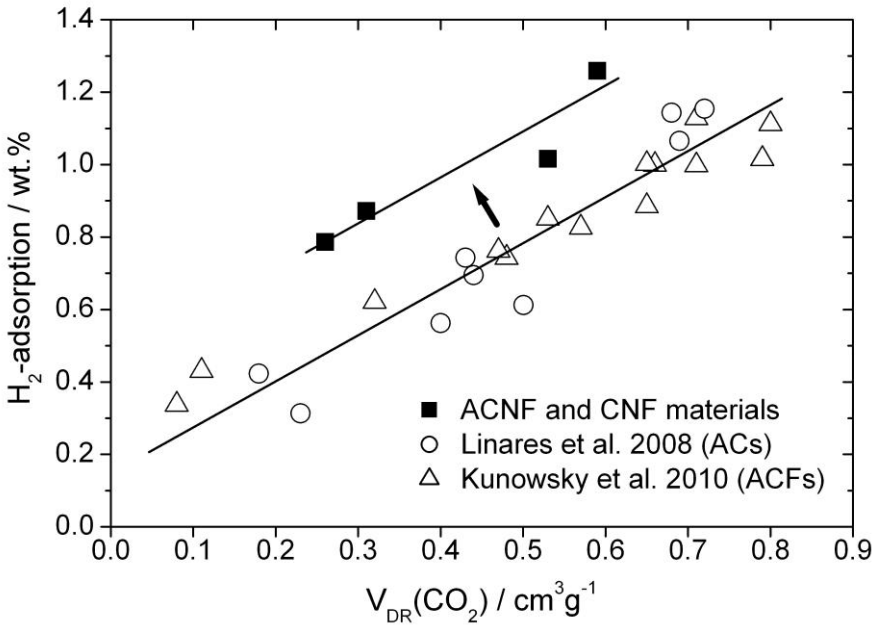

Figure 9. H_2 excess adsorption at 298 K and 20 MPa over narrow microporosity for different carbon materials, measured in the same device. Values for activated carbons (ACs) and activated carbon fibers (ACFs) were taken from [24] and [27], respectively.

temperature and 20 MPa) other remarkable hydrogen adsorption amounts above 1 wt.% have been published [24, 27, 35-37, 43-45]; however, none of them are related to carbon nanofiber materials.

The relation between hydrogen uptake and $V_{DR}(CO_2)$ can be seen in Figure 9, where the maximum adsorption capacities of hydrogen adsorption at room temperature and 20 MPa are plotted versus the samples' narrow micropore volumes. The filled symbols correspond to the samples investigated in this study (isotherms in Figure 8). For comparison purpose, results which were previously published by our research group are included in the graph, represented by empty symbols [24, 27]. The previous adsorption amounts were obtained for activated carbons (circles) [24] and activated carbon fibers

(triangles) [27]. The fact that the same sample characterization (CO_2 at 273 K) and the same experimental setup, procedure and equipment were used for all of the measurements ensures a high comparability among all of the results plotted in Figure 9. Surprisingly, and different to what has been seen in Figure 7b, the results obtained by the CNF-based materials at room temperature are superior to other activated carbon adsorbents. Such different behavior among carbon materials has not been reported before and hence it needs further work to understand its origin. Anyway, this difference at room temperature seems to indicate that these CNF-based materials may have very narrow microporosity, accessible to H_2 at room temperature but not to CO_2. The different kinetic molecular diameters of both gases (0.24 nm for H_2 vs. 0.33 nm for CO_2) could be the reason. At 77 K, where the kinetic adsorption energy of H_2 is much lower than at room temperature, both gases present similar accessibilities.

For hydrogen storage application, the total storage capacity is the most important issue. Thereby, not only the H_2 molecules that are adsorbed in the porosity are taken into account, but also the hydrogen gas which is compressed in the void space of the tank volume [24, 27, 35, 46]. For the best sample (ACNF-CD24), a total hydrogen storage capacity of 17.4 $g(H_2)\ l^{-1}$ has been calculated, taking a skeleton density of 2.22 $g\ cm^{-3}$ and a packing density of 0.49 $g\ cm^{-3}$. It has to be recalled that such a high packing density is achieved by keeping the sample under pressure in the mechanical press. Using a more realistic packing density after pressure release (0.21 $g\ cm^{-3}$, see Table 1), the total H_2 storage capacity decreases to 15.6 $g(H_2)\ l^{-1}$. As it was mentioned earlier, from an application point of view, it is desirable to retain a high density. This can be achieved, either by maintaining the mechanical pressure, or, as it has been demonstrated above, by preparing mechanically resistant monoliths from the ACNFs. In the case of

the monolith prepared from sample ACNF-CD24, the monolith density decreases only slightly to 0.46 g cm^{-3} in comparison with the original ACNFs, for which the mechanical pressure is maintained. Thanks to this high density, and despite the partial loss of porosity in comparison with its pristine ACNFs, the ACNF-CD24-M monolith reaches a high total H_2 storage capacity of 15.8 g(H_2) l^{-1}, a value higher than for the uncompacted ACNF-CD24 sample, never published before for ACNF materials.

4. Conclusions

The investigated amorphous nanofibers (CNFs), produced by the polymer blend technique, are very easily activated by CO_2. With these CNF-precursors, highly specialized adsorbents (ACNFs) can be prepared, as well as monolith materials from both, the pristine CNFs and ACNFs. The obtained ACNFs have a high compressibility and, consequently, a high packing density under mechanical pressure which is preserved upon monolith synthesis. Additionally, CO_2 activation of these CNFs, in relation to other activating agents (steam activation and chemical activation with alkaline hydroxides), renders suitable yields and results advantageous to develop and control the sample narrow micropores volumes (< 0.7 nm), contrarily to what happens for most other precursors. The hydrogen storage at 77 K (up to 0.11 MPa) and at room temperature (up to 20 MPa) on these CNF materials show that in both cases, H_2 uptake depends on the volume of narrow micropores (< 0.7 nm) of the sample. The comparison study carried out with other activated carbon materials having different morphologies and dimensional sizes shows that at 77 K all the compared samples behave similarly. However, at room temperature and 20 MPa, the ACNFs behave much better than any of

the other carbon materials. ACNFs reaching a H_2 adsorption capacity of around 1.3 wt.% are prepared, as well as its monolith with a suitable mechanical resistance that reaches also a remarkable value (1 wt.%). In terms of total hydrogen storage the ACNFs reach 17.4 g(H_2) l^{-1} and its monolith 15.8 g(H_2) l^{-1}.

Acknowledgements

The authors thank the Spanish MICINN (Project MAT2009-07150) and Generalitat Valenciana and FEDER (project PROMETEO/2009/047) for financial support.

References

[1] Lee K, Zhang J, Wang H, Wilkinson DP. Progress in the synthesis of carbon nanotube- And nanofiber-supported Pt electrocatalysts for PEM fuel cell catalysis. J Appl Electrochem 2006; 36(5):507−22.

[2] Zaragoza-Martín F, Sopeña-Escario D, Morallón E, Salinas-Martínez de Lecea C. Pt/carbon nanofibers electrocatalysts for fuel cells. Effect of the support oxidizing treatment. J Power Sources 2007; 171:302−9.

[3] Su DS, Schlögl R. Nanostructured carbon and carbon nanocomposites for electrochemical energy storage applications. ChemSusChem 2010; 3:136−68.

[4] Endo M, Kim YA, Hayashi T, Nishimura K, Matusita T, Miyashita K, et al. Vapor-grown carbon fibers (VGCFs) – basic properties and their battery applications, Carbon 2001; 9:1287−97.

[5] Shiraishi S, Kurihara H, Ida Y, Oya A. Preparation of highly porous carbon nanofibers by polymer blend technique and its electric double layer capacitance, Extended Abstract, Carbon'03. In: An international conference on carbon. Oviedo (Spain): Spanish Carbon Group, 2003; p. 211−4.

[6] Shiraishi S, Miyauchi T, Sasaki R, Nishina N, Oya A, Hagiwara R. Electric double layer capacitance of activated carbon nanofibers in ionic liquid: $EMImBF_4$, Electrochemistry 2007, 75(8):619-21.

[7] Kim C. Electrochemical characterization of electrospun activated carbon nanofibers as an electrode in supercapacitors. J Power Sources 2005; 142(1−2):382−8.

[8] Barranco V, Lillo-Ródenas MA, Linares-Solano A, Oya A, Pico F, Ibañez J, et al. Amorphous carbon nanofibers and their activated carbon nanofibers as supercapacitor electrodes. J Phys Chem C 2010; 114(22):10302−7.

[9] Rodriguez NM, Chambers A, Baker RTK. Catalytic Engineering of Carbon Nanostructures. Langmuir 1995; 11:3862−6.

[10] Taboada CD, Batista J, Pintar A, Levec J. Preparation, characterization and catalytic properties of carbon nanofiber-supported Pt, Pd, Ru monometallic particles in aqueous-phase reactions. Appl Catal B 2009; 89(3-4):375−82.

[11] Mauter MS, Elimelech M. Environmental applications of carbon-based nanomaterials. Environ Sci Technol 2008; 42(16):5843−59.

[12] Kang I, Heung YY, Kim JH, Lee JW, Gollapudi R, Subramaniam S, et al. Introduction to carbon nanotube and nanofiber smart materials. Composites Part B: Engineering 2006; 37(6):382−94.

[13] Ahn CC, Ye Y, Ratnakumar BV, Witham C, Bowman Jr RC, Fultz B. Hydrogen desorption and adsorption measurements on graphite nanofibers. Appl Phys Lett 1998; 73(23):3378−80.

[14] Chambers A, Park C, Baker RTK, Rodriguez NM. Hydrogen storage in graphite nanofibers. J Phys Chem B 1998; 102(22):4253−6.

[15] Fan YY, Liao B, Liu M, Wei YL, Lu MQ, Cheng HM. Hydrogen uptake in vapor-grown carbon nanofibers. Carbon 1999; 37(10):1649−52.

[16] Tibbetts GG, Meisner GP, Olk CH. Hydrogen storage capacity of carbon nanotubes, filaments, and vapor-grown fibers. Carbon 2001; 39:2291−301.

[17] Züttel A, Sudan P, Mauron Ph, Kiyobayashi T, Emmenegger Ch, Schlapbach L. Hydrogen storage in carbon nanostructures. Int J Hydrogen Energy 2002; 27(2):203−12.

[18] Hirscher M, Becher M, Haluska M, Quintel A, Skakalova V, Choi YM, et al. Hydrogen storage in carbon nanostructures. J Alloys Compd 2002; 330−332:654−8.

[19] Rzepka M, Bauer E, Reichenauer G, Schliermann T, Bernhardt B, Bohmhammel K, et al. Hydrogen storage capacity of catalytically grown carbon nanofibers. J Phys Chem B 2005; 109:14979−89.

[20] Blackman JM, Patrick JW, Arenillas A, Shi W, Snape CE. Activation of carbon nanofibres for hydrogen storage. Carbon 2006; 44(8):1376−85.

[21] Im JS, Park SJ, Kim TJ, Kim YH, Lee YS. The study of controlling pore size on electrospun carbon nanofibers for hydrogen adsorption. J Colloid Interface Sci 2008; 318:42−9.

[22] Suárez-García F, Vilaplana-Ortego E, Kunowsky M, Kimura M, Oya A, Linares-Solano A. Activation of polymer blend carbon nanofibers by alkaline hydroxides and their hydrogen storage performances. Int J Hydrogen Energy 2009; 34(22):9141-50.

[23] Darkrim Lamari F, Weinberger B, Kunowsky M, Levesque D. Material design using molecular modeling for hydrogen storage. AIChE J 2009; 55(2):538−47.

[24] Linares-Solano A, Jordá-Beneyto M, Kunowsky M, Lozano-Castelló D, Suárez-García F, Cazorla-Amorós D. Hydrogen storage in carbon materials. In: Terzyk AP, Gauden PA, Kowalczyk P, editors. Carbon materials - theory and practice. Kerala: Research Signpost; 2008, p. 245−81.

[25] Suzuki M. Activated carbon fiber: Fundamentals and applications. Carbon 1994, 32(4):577−86.

[26] Inagaki M. New carbons: control of structure and functions. 1st ed. Kidlington, Oxford: Elsevier; 2000.

[27] Kunowsky M, Marco-Lozar JP, Cazorla-Amorós D, Linares-Solano A. Scale-up activation of carbon fibres for hydrogen storage. Int J Hydrogen Energy 2010; 35:2393−402.

[28] Oya A, Kasahara N. Preparation of thin carbon fibers from phenol-formaldehyde polymer micro-beads dispersed in polyethylene matrix. Carbon 2000; 38:1141−4.

[29] Hulicova D, Oya A. The polymer blend technique as a method for designing fine carbon materials. Carbon 2003; 41:1443−50.

[30] Chung GS, Jo SM, Kim BC. Properties of carbon nanofibers prepared from electrospun polyimide. J Appl Polym Sci 2005; 97:165−70.

[31] Yang Y, Mei-Hua Z, Gang X, Zheng-Xiong J. Preparation and characterization of PAN-based ultra-fine activated carbon fiber adsorbent. J Porous Mater 2011; 18(3), 379−87.

[32] Kyotani T, Tsai L, Tomita A. Preparation of ultrafine carbon tubes in nanochannels of an anodic aluminum oxide film. Chem Mater 1996; 8(8):2109−13.

[33] Lozano-Castelló D, Cazorla-Amorós D, Linares-Solano A, Quinn DF. Activated carbon monoliths for methane storage: influence of binder. Carbon 2002; 40:2817–25.

[34] Gadea-Ramos E, Suárez-García F, Cazorla-Amorós D, Jordá-Beneyto M, Linares-Solano A. Method and equipment for measuring the high-pressure sorption isotherms of supercritical fluids and gases. International Patent WO 2008/107505 (A1), 2008.

[35] Jordá-Beneyto M, Suárez-García F, Lozano-Castelló D, Cazorla-Amorós D, Linares-Solano A. Hydrogen storage on chemically activated carbons and carbon nanomaterials at high pressures. Carbon 2007; 45(2):293–303.

[36] Kunowsky M, Weinberger B, Lamari Darkrim F, Suárez-García F, Cazorla-Amorós D, Linares-Solano A. Impact of the carbonisation temperature on the

activation of carbon fibres and their application for hydrogen storage. Int J Hydrogen Energy 2008; 33(12):3091–5.

[37] Kunowsky M, Suárez-García F, Cazorla-Amorós D, Linares-Solano A. Synthesis of activated carbon fibers for high-pressure hydrogen storage. Ceramic Transactions 2009; 202:69–75.

[38] Linares-Solano A, Lozano-Castelló D, Lillo-Ródenas MA, Cazorla-Amorós D, Carbon activation by alkaline hydroxides: preparation and reactions, porosity and performances. Chem Phys Carbon 2008; 30:1−62.

[39] Ahmadpour A, Do D. The preparation of active carbons from coal by chemical and physical activation. Carbon 1996; 34:471−9.

[40] Agarwal RK, Schwarz JA. Analysis of high pressure adsorption of gases on activated carbon by potential theory. Carbon 1988; 26(6):873−87.

[41] Dubinin MM. Physical adsorption of gases and vapors in micropores. In: Cadenhead DA, Danielli JF, Rosenberg MD, editors. Progress in Surface and Membrane Science. New York: Academic Press; 1975, p. 1−70.

[42] Thomas KM. Hydrogen adsorption and storage on porous materials. Catalysis Today 2007; 120(3–4):389–98.

[43] de la Casa-Lillo MA, Lamari-Darkrim F, Cazorla-Amorós D, Linares-Solano A. Hydrogen storage in activated carbons and activated carbon fibers. J Phys Chem B 2002, 106:10930−4.

[44] Nishihara H, Hou PX, Li LX, Ito M, Uchiyama M, Kaburagi T, et al. High-pressure hydrogen storage in zeolite-templated carbon. J Phys Chem C 2009, 113(8):3189–96.

[45] Fierro V, Szczureka A, Zloteac C, Marêchéa JF, Izquierdod MT, Albiniakb A, et al. Experimental evidence of an upper limit for hydrogen storage at 77 K on activated carbons. Carbon 2010, 48(7):1902−11.

[46] Zhou L, Zhou Y, Sun Y. Enhanced storage of hydrogen at the temperature of liquid nitrogen. Int J Hydrogen Energy 2004; 29(3):319−22, 2004.